Borden et al.[5] are due to the two different formalisms used to treat open-shell systems.

Acknowledgment. I thank Professor S. F. Nelsen for helpful discussions and Professor W. T. Borden for communicating his results on this system prior to publication. Thanks are due to the staff of the Regionales Rechenzentrum Erlangen for their cooperation.

Registry No. $P_2H_4^{+\cdot}$, 86676-97-3.

Theoretical Electron Deformation Density Studies on Chromium Benzene Tricarbonyl

Randall A. Kok and Michael B. Hall*

Contribution from the Department of Chemistry, Texas A&M University, College Station, Texas 77843. *Received September 4, 1984*

Abstract: Theoretical calculations on the electron density distribution of chromium benzene tricarbonyl are reported. A new method of including thermal smearing into static deformation density maps is used to produce theoretical dynamic deformation density maps of chromium benzene tricarbonyl which are directly compared to experimental maps. This comparison shows that a number of problems remain in the experimental electron deformation density of this complex. The changes in the electron distribution around the chromium are inconsistent with the theoretical deformation density maps and seem to be too large to be explained as an effect that would result from thermal smearing. Also the pattern of electron gain and loss around the chromium in one experimental study is difficult to explain in simple chemical terms and suggests that perhaps these peaks may be representative of the "ghost peaks" found by other researchers. This study shows that accurate calculations can aid in the interpretion of experimental deformation densities.

Recently, there has been increasing interest in studying electron density distributions, both experimentally and theoretically. Improved experimental design and low-temperature crystal structures have together increased the accuracy of electron densities determined by X-ray diffraction methods. Electron density distributions determined theoretically have also improved due to faster computers. As a result, the number of studies comparing theoretical and experimental electron density distributions has increased significantly.[1-11] The quality of both experiment and theory now provides the opportunity to quantitatively compare the two as a way of checking the reliability of both approaches.

In order to compare directly experimental and theoretical electron density distributions, one must take into account the effect of thermal smearing of the experimental density. A growing number of papers have examined this problem and have proposed ways to incorporate thermal smearing into their theoretical maps.[12-14] Up to now most of the molecules chosen for comparison have consisted of only light atoms. In this paper we report the first study that compares theoretical static and dynamic deformation densities with experimental electron density distributions for a transition-metal complex. We also report a new and simple technique for incorporating thermal smearing into the theoretical charge distribution that compares favorably with previously reported techniques. We have verified our thermal smearing technique by comparing our result for the formate ion with calculations reported by Fuess and co-workers.[15] The transition-metal complex we have studied theoretically is chromium benzene tricarbonyl, $Cr(C_6H_6)(CO)_3$. Experimental deformation densities on this compound were first reported in a pioneering study by Rees and Coppens[16] in 1973. This study was the first low-temperature X-ray crystal determination of a transition-metal complex, and in this study deformation densities of the benzene and carbonyl planes were reported. We will be comparing our theoretical results with this experimental study as well as with more recent work done at the Molecular Structure Corp. by Troup and Extine.[17]

Although a theoretical electron density distribution study including thermal smearing on a transition-metal complex has not yet been reported, numerous experimental studies of electron density distributions in transition-metal complexes have been reported.[18-25] These studies illustrate several problems in experimentally determined electron density distributions. First, the presence of chemically unreasonable electron density features around metal atoms and metal–ligand bonding regions have been

(1) Ruysink, A. F. J.; Vos, A. *Acta Crystallogr., Sect. A* **1974**, *A30*, 497.
(2) Bats, J. W.; Feil, D. *Chem. Phys.* **1977**, *22*, 175.
(3) De With, G. *Chem. Phys.* **1978**, *32*, 11.
(4) Benard, M. *J. Am. Chem. Soc.* **1978**, *100*, 7740.
(5) Stevens, E. D. *Acta Crystallogr. Sect. B* **1980**, *B36*, 1876.
(6) Benard, M.; Coppens, P.; DeLucia, M. L.; Stevens, E. D. *Inorg. Chem.* **1980**, *19*, 1924.
(7) Mitschler, A.; Rees, B.; Wiest, R.; Benard, M. *J. Am. Chem. Soc.* **1982**, *104*, 7501.
(8) Breitenstein, M.; Dannohl, H.; Meyer, H.; Schweig, A.; Zittlau, W. In "Electron Distributions and the Chemical Bond"; Coppens, P., Hall, M. B., Eds.; Plenum Press: New York, 1982; p 255.
(9) Heijser, W.; Baerends, E. J.; Ros, P. *Discuss. Faraday Soc. (Symp.)* **1980**, *14*, 211.
(10) Leung, P. C.; Coppens, P. *Acta Crystallogr., Sect. B* **1983**, *B39*, 535.
(11) Kutzler, F. W.; Swepston, P. N.; Berkovitch-Yellin, Z.; Ellis, D. E.; Ibers, J. A. *J. Am. Chem. Soc.* **1983**, *105*, 2296.
(12) Hase, H.; Reitz, H.; Schweig, A. *Chem. Phys. Lett.* **1976**, *39*, 157.
(13) Coppens, P.; Stevens, E. D. *Isr. J. Chem.* **1977**, *16*, 175.
(14) Stevens, E. D.; Rys, J.; Coppens, P. *Acta Crystallogr. Sect. A* **1977**, *A33*, 333.
(15) Fuess, H.; Bats, J. W.; Dannohl, H.; Meyer, H.; Schweig, A. *Acta Crystallogr. Sect. B* **1982**, *B38*, 736.
(16) Rees, B.; Coppens, P. *Acta Crystallogr., Sect. B* **1973**, *B29*, 2515.
(17) Troup, J. M.; Extine, M. W., unpublished results.
(18) Iwata, M.; Saito, Y. *Acta Crystallogr., Sect. B* **1973**, *B29*, 822.
(19) Wang, Y.; Coppens, P. *Inorg. Chem.* **1976**, *15*, 1122.
(20) Stevens, E. D.; Coppens, P. *Acta Crystallogr., Sect. B* **1980**, *B36*, 1864.
(21) Coppens, P. *Trans. Am. Crystallogr. Assoc.* **1980**, *16*, 59.
(22) Martin, M.; Rees, B.; Mitschler, A. *Acta Crystallogr., Sect. B* **1982**, *B38*, 6.
(23) Troup, J. M.; Extine, M. W.; Ziolo, R. F. In "Electron Distributions and the Chemical Bond"; Coppens, P., Hall, M. B., Eds.; Plenum Press: New York, 1982; p 285.
(24) Goddard, R.; Kruger, C. In "Electron Distributions and the Chemical Bond"; Coppens, P., Hall, M. B., Eds.; Plenum Press: New York, 1982; p 297.
(25) Ziolo, R. F.; Troup, J. M. *J. Am. Chem. Soc.* **1983**, *105*, 229.

0002-7863/85/1507-2599$01.50/0

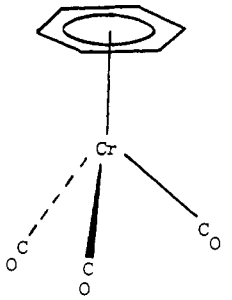

Figure 1. Structure of $Cr(C_6H_6)(CO)_3$. The three carbonyl ligands have been averaged to give the geometry shown. Carbon–carbon bonds alternate between 1.423 and 1.406 Å around the benzene ring. H atoms are below the plane of the benzene by 0.032 Å. The center of the benzene ring to the Cr distance is 1.728 Å. The distance from the Cr to the C of the carbonyl is 1.845 Å, and the C–O bond distance is 1.157 Å. The angle from the center of the benzene ring through the Cr to the carbonyl is 126.52°.

reported by several researchers.[10,16,21,23] Several possible reasons for these features have been proposed, including thermal stress,[23] inadequate absorption correction,[26] and inadequate quality in the crystal structure data set.[11] Second, features that are expected in the electron density distribution maps are often not present. For example, studies on $Mn_2(CO)_{10}$ indicated very little density buildup between the metal atoms.[22] Even when prepared $Mn(CO)_5$ fragments are subtracted, the peak in the theoretical deformation map is only 0.10 e Å^{-3}.[9] Studies on dichromium tetraacetate dihydrate also indicate a very small buildup of electron density in the Cr–Cr bonding region.[6] Another example is the electron density around lone pairs of electrons. Often in electron density distributions of carbonyls in metal complexes the electron density has disappeared completely from the oxygen lone-pair region.[10,16]

Although we cannot yet explain all these problems, we will show in this paper how theoretical calculations can be used along with experiment to help guide both experimentalists and theoreticians to a better understanding of electron density distributions.

Theory

Geometry. The geometry of $Cr(C_6H_6)(CO)_3$ is shown in Figure 1 and was based on the X-ray and neutron crystal structure reported by Rees and Coppens.[16] Although the crystal structure contains a mirror plane creating two different kinds of carbonyls, we have averaged the bond lengths to give the theoretical calculation C_{3v} symmetry. In accordance with the neutron crystal structure, the hydrogens in this calculation are no longer in the plane of the carbon atoms in benzene but are bent toward the Cr atom by about 0.03 Å. Also, the C–C bonds in benzene are no longer equal but rather alternate between long and short bonds, the long bonds being the ones eclipsing the axes of the carbonyls.

Basis. The basis functions employed in this study were obtained from a least-squares fit of a linear combination of Gaussians to near-Hartree–Fock-quality Slater-type functions.[27-29] The program GEXP processes the functions from the 1s outward, keeping each orbital of higher n quantum number orthogonal to the previous ones. This procedure results in an efficiently nested representation of the function.[30] In this study, the number of Gaussians used for each function was increased until the integral error of the fitting[31] was less than 3×10^{-4} for valence functions and 6×10^{-4} for core functions. It was found that three Gaussians per atomic orbital were sufficient for most core orbitals. Four Gaussians were used for the H 1s and the C and O 2p, and five Gaussians were necessary to fit the Cr 3d.

For the carbon and oxygen atoms, the most diffuse component of the valence p function was split off to form a double-ζ representation. For the chromium atom, the two most diffuse components of 3d orbital were split off to form a triple-ζ representation. Also two extra s functions with exponents of 0.15 and 0.05 and two extra p functions with exponents of 0.21 and 0.07 were added to the basis, resulting in a set of (11s 8p 5d) primitive GTOs contracted to [5s 4p 3d].

Table I. Comparison of Static and Dynamic Deformation Density Peak Heights[a] for the Formate Ion

molecular region	static[b]	dynamic[b]	static[c]	dynamic[c]
C–H	0.80	0.45	1.00	0.80
C–O	0.70	0.55	0.70	0.50
O lone pair	0.95	0.45	1.00	0.50

[a] In e Å^{-3}. [b] Reference 15. [c] This work.

Calculations. All calculations were carried out on the Texas A&M University Amdahl 470V/6 and V/7 computers and the Department of Chemistry's VAX 11/780 computer. The integrals and the Hartree–Fock–Roothaan[32] calculations were done with the ATMOL3 system of programs.[33] The wave functions were used in the program MOPLOT[34] to generate total electron density maps of both the complex and its component fragments. The fragment maps were summed together, and that sum was subtracted from the total density of the complex to yield the fragment deformation density. These maps were drawn with the program CONTOUR[35] on a Xerox 9700 electronic printing system with the graphics package called Electronic Printer Image Construction.

Theoretical Dynamic Deformation Density Maps. We have employed a new technique for including the effect of thermal smearing in the theoretical deformation density maps. A theoretical calculation of the static deformation density provides a picture of the electron distribution at the instant when the atoms all occupy their normal equilibrium positions. However, when the atom moves out of its equilibrium position, the electron density distribution in the original plane changes. If one were to move all the atoms according to their vibrational motions and continue calculating the deformation density, you would get a series of "snapshots" of the changing electron density distribution. Of course in practice one cannot get an instantaneous picture of the electrons. Rather an average of all the possible distributions emerges. This same result is achieved theoretically by averaging the series of "snapshots" that you calculate as you shift the atoms. This method is appropriate since most of the motion of the molecule in a crystal is librational and translational, that is the molecule as a whole shifts.

We have chosen this approach to calculate a theoretical dynamic deformation density. We used the 50% probability ellipsoids to define a surface inside of which the atoms spend one-half their time. We then calculated the average size of the 50% probability ellipsoids for the atoms and chose four points in a tetrahedral pattern on the surface of the ellipsoid. These four static deformation density maps were then averaged to give a theoretical dynamic deformation density. We also repeated the procedure with a set of six points in an octahedral pattern, which would seem preferable since this centrosymmetric pattern would correspond better to the dominate harmonic thermal motion. However, after averaging the six resulting static density maps we found that they gave the same result. Also, the same results were obtained for various choices of the four-point pattern. Small differences near the nuclei did appear when one or more of the points was chosen in the original plane. In the reported maps two points above and two points below the plane were chosen. This technique includes primarily translational motion; librational motion could be included by averaging in maps in which the molecule was rotated instead.

We tested this technique on the formate ion, $COOH^-$, an anion on which other theoretical smearing techniques have been employed.[15] We calculated the total density in the same basis set used by Fuess and co-workers[36,37] and chose four points to use in calculating the dynamic density maps. A spherical ellipsoid of radius 0.19 Å with a standard deviation of 0.05 Å was determined by averaging the principal radii of all thermal ellipsoids including those of H. The resulting static and dynamic deformation density maps are shown in Figure 2. Table I

(26) Coppens, P. *ACA Program Abstr. Ser. 2.* **1982**, *10*, 25.
(27) Clementi, E. *J. Chem. Phys.* **1964**, 40.
(28) Clementi, E. *IBM J. Res. Dev.* **1965**, *9*, 2 (and its supplement, "Tables of Atomic Functions").
(29) Roetti, C.; Clementi, E. *J. Chem. Phys.* **1974**, *60*, 3342.
(30) Marron, M. T.; Handy, M. C.; Parr, R. G.; Silverstone, H. G. *Int. J. Quantum Chem.* **1970**, *4*, 245.
(31) Stewart, R. F. *J. Chem. Phys.* **1970**, *52*, 431.
(32) Roothaan, C. C. J. *Rev. Mod. Phys.* **1951**, *23*, 69.
(33) Hillier, I. H.; Saunders, V. R.; Guest, M. F. ATMOL3 System; Chemistry Department, University of Manchester, Manchester, U.K., and SRC Laboratory, Daresbury, U.K.
(34) Lichtenberger, D. L. Ph.D. Dissertation, University of Wisconsin, Madison, WI, 1974. Program available from Quantum Chemistry Program Exchange, Indiana University, Bloomington, IN 47401, Program No. 284.
(35) An in-house program that uses CONREC, a special smoothing routine for drawing contours, developed at the National Center for Atmospheric Research (NCAR), Boulder, CO, and adapted for use on the Amdahl 470V/6 by Thomas Reid, Data Processing Center, Texas A&M University.
(36) Ditchfield, R.; Hehre, W. J.; Pople, J. A. *J. Chem. Phys.* **1971**, *54*, 724.
(37) Hase, H.; Schweig, A. *Angew. Chem., Int. Ed. Engl.* **1977**, *16*, 258.

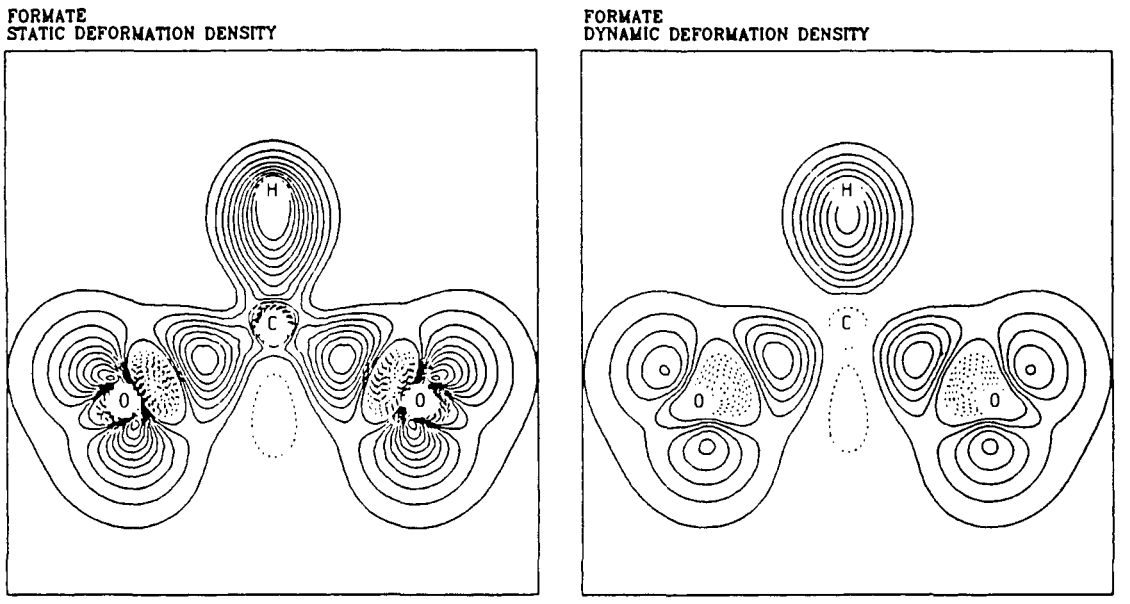

Figure 2. Static and dynamic deformation density maps for the formate ion. The contour interval is 0.1 $eÅ^{-3}$ and negative contours are broken in all maps. The left map represents the difference between the total electron density and spherical ground-state atomic densities. The right map represents dynamic deformation density produced by incorporating thermal smearing into the static deformation density map.

contains a comparison of the peak heights determined in the previous study by Fuess and co-workers with the peak heights obtained by our technique. The results indicate that our technique reproduces the effect of thermal smearing in the carbon–oxygen region, although there are some differences in the C–H bond region. This is due to the larger thermal motion of the H atom, which is accounted for more completely in the method of Hase, Reitz, and Schweig.[12]

Results and Discussion

Theoretical Deformation Densities. The theoretical deformation density maps for $Cr(C_6H_6)(CO)_3$ are shown in Figure 3. The top two maps show the electron density distribution in a plane containing all the carbon atoms of the benzene ring. The bottom two maps show the electron density distribution in a plane which contains the chromium atom and one carbonyl group and which cuts through the middle of two of the carbon–carbon bonds in the benzene ring. At the left side of Figure 3, the static deformation densities are plotted. These were generated by subtracting spherical ground-state atoms in the same basis set from the total electron density of the molecule. This map shows the changes in electron density which occur when forming the molecule from its constituent atoms. On the right side of Figure 3, the theoretical dynamic deformation densities are plotted. These were determined from a series of static maps with the technique described in the Theory section. A spherical ellipsoid of radius 0.17 Å with a standard deviation of 0.03 Å was determined by averaging the principal radii of all thermal ellipsoids except those of H.

In the top maps, one can see electron deformation densities typical of benzene rings with electron density buildup in the middle of the carbon–carbon bond and between the carbons and hydrogens and electron density loss outside the hydrogens. In the bottom maps, several important features are noteworthy. First, there is significant buildup of electron density on the side of the oxygen opposite the oxygen–carbon bond and between the carbon and the chromium where the lone pairs for the carbon and the oxygen atoms would be located. There is electron density gain on the carbon side of the C–O bond but loss on the oxygen side of the C–O bond. There is also loss off the C–O axis "above" and "below" the carbon. This pattern of electron density around a carbonyl group has been found by other researchers, both experimental and theoretical.[38,39]

The theoretical dynamic density probably overemphasizes the gain in the O lone-pair region for two reasons. One, our average thermal parameter, is smaller than the O thermal parameter. Two, the librational motion or oxygen wag, which is very effective in smearing the O lone pair, has not been explicitly included in our procedure. Larger basis sets on C and O would increase the buildup of density in the C–O bond.[39] Thus, in the C–O bond region our dynamic density increase is probably too small. In general, the electron density is underestimated in the bonding regions and overestimated in the lone-pair regions at this level of calculation.

Table II. Comparison of Deformation Density Peak Heights[a] for $Cr(C_6H_6)(CO)_3$

molecular region	theoretical static	theoretical dynamic[b]	Rees and Coppens[c]	Troup and Extine[d]
		Benzene Plane		
C–C	0.40	0.30	0.40	0.40
		Carbonyl Plane		
Cr	1.00	0.70	0.95	0.05
C lone pair	0.90	0.70	0.40	0.35
C–O	0.30	0.20	0.50	0.40
O lone pair	0.80	0.60	0.45	0.15

[a] In e $Å^{-3}$. [b] This work. [c] Reference 16. [d] Reference 17.

Around the chromium atom the electron density has an eight-lobe arrangement with four lobes of electron density gain at 90° from each other separated by four lobes of electron density loss also at 90° from each other but offset from the positive lobes by 45°. Notice that the negative lobes point directly toward the carbon–carbon bonds of the benzene ring while the positive lobe points up toward the center of the benzene ring. This can be explained by simple crystal field theory if one assumes the benzene ring is taking up three coordination sites on the octahedral chromium atom. As the ligands approach, electron density flows out of the d orbitals pointed directly toward the incoming ligands into d orbitals pointed between the incoming ligands. After correcting the static maps for thermal motion, the main features of the maps are unchanged. In both planes, the main effect of the thermal motion is to reduce the number of contours throughout the maps as you go from static to dynamic. Since the Cr thermal parameter is small, a more sophisticated treatment of the thermal motion is unlikely to change the dynamic density. Comparison of these results with calculations in smaller basis sets suggests that these results are stable with respect to improvements in the basis set. Thus, the region around the Cr is likely to be the most accurate region of our maps.

Comparison with Experiment. Table II compares the peak heights for the static and dynamic theoretical deformation density

(38) Rees, B.; Mitschler, A. *J. Am. Chem. Soc.* **1976**, *98*, 7918.
(39) Sherwood, D. E., Jr.; Hall, M. B. *Inorg. Chem.* **1983**, *22*, 93.

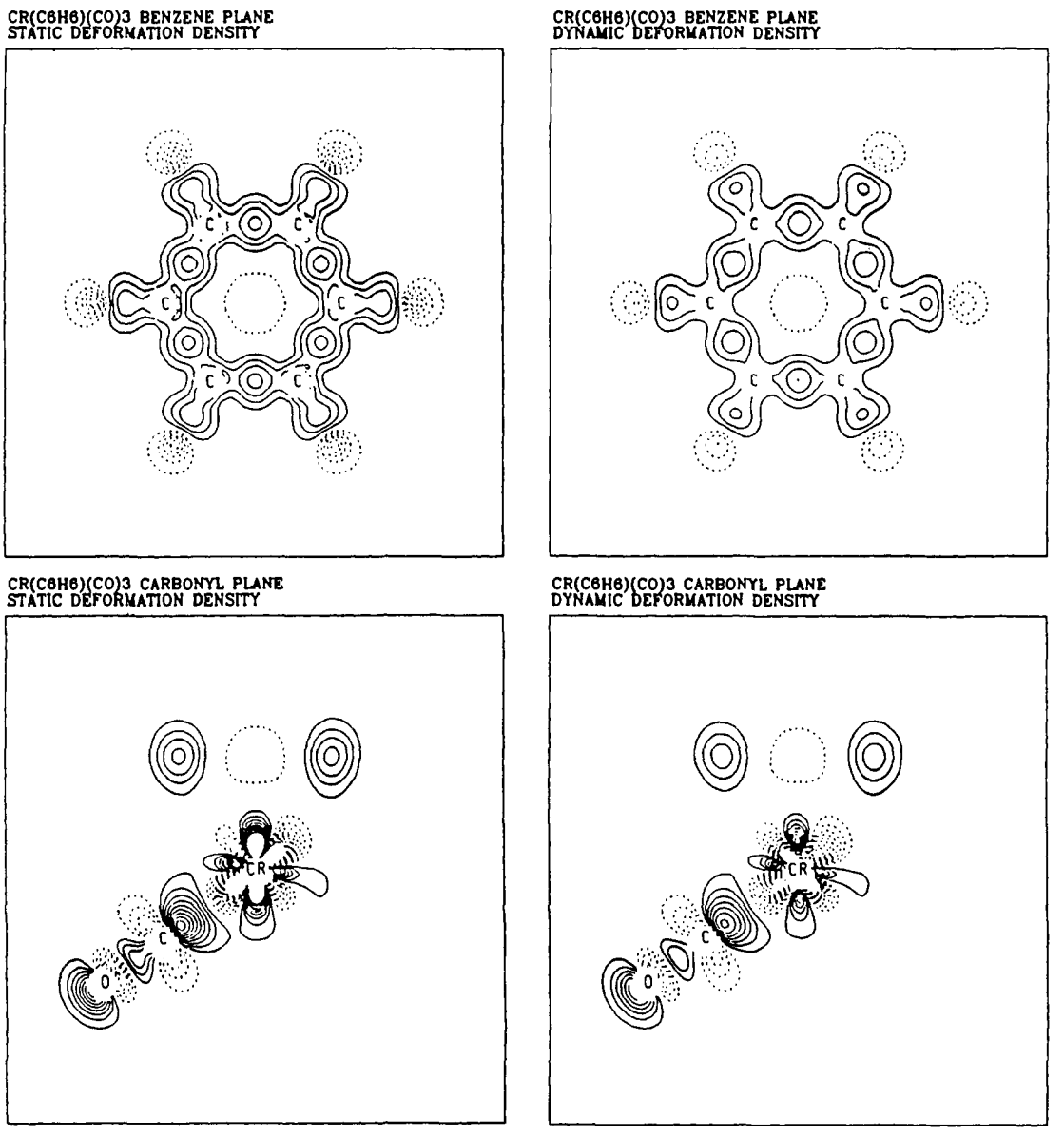

Figure 3. Static and dynamic deformation density maps for $Cr(C_6H_6)(CO)_3$. The top two maps show the electron density distribution in a plane containing the benzene ring while the bottom maps show the density in a plane containing the chromium and one carbonyl group. The left-hand maps represent static deformation densities while the right-hand maps represent the dynamic deformation densities.

maps with the experimental deformation density maps from the original low-temperature X-ray crystal structure work done by Rees and Coppens[16] and with more recent low-temperature work done at the Molecular Structure Corporation by Troup and Extine.[17] Plots of the deformation density obtained by these two studies is shown in Figure 4. Note that, while our maps are contoured at 0.10 e $Å^{-3}$, the Rees and Coppens maps are contoured at 0.15 e $Å^{-3}$ and the Troup and Extine maps are contoured at 0.05 e$Å^{-3}$. It is immediately clear that important differences exist between the theoretical and experimental electron density distributions. First we will compare the theoretical deformation densities with those of Rees and Coppens and then with those of Troup and Extine.

The agreement between the theoretical and experimental deformation densities of Rees and Coppens in the plane containing the benzene ring is quite good. In the plane containing the carbonyl group, however, several large differences are noticeable. First in the carbonyl region, the electron density of the oxygen lone pair is lower and the carbon–oxygen bond is higher when compared to the theoretical deformation density. Second, large differences occur in the region right around the chromium atom. In the theoretical maps, there is an eightfold pattern of positive and negative lobes, whereas in the experimental maps only a fourfold pattern is seen. This pattern has alternating positive and negative lobes at about 90° from each other and oriented so that one positive lobe and one negative lobe are pointing directly at the carbon–carbon bond of the benzene ring. This pattern is difficult to explain in chemical terms. Third, the three carbonyl groups are not equivalent in the crystal structure even though they are equivalent by molecular symmetry. The number of contours in the oxygen–carbon bond region changes by two contours while the number of contours around the chromium atom changes by five contours when going from the plane containing one carbonyl to the plane containing the other carbonyl. Equally disturbing is that the pattern around the Cr appears to have rotated in the other plane so that the two planes are also in qualitative disagreement. In spite of these differences, the average maximum density and distance of the maximum from the chromium atom are similar to those of our theoretical maps.

When comparing the theoretical deformation densities with those of Troup and Extine, the features in the benzene plane are once more similar. Again a comparison of the carbonyl plane shows larger differences. Here, as in the work by Rees and Coppens, the deformation density in the oxygen lone-pair region is smaller, while that in the carbon–oxygen bonding region is larger, when compared to the theoretical maps. Around the chromium atom the electron density is gone almost completely. The electron density gain, that is there, points toward the center

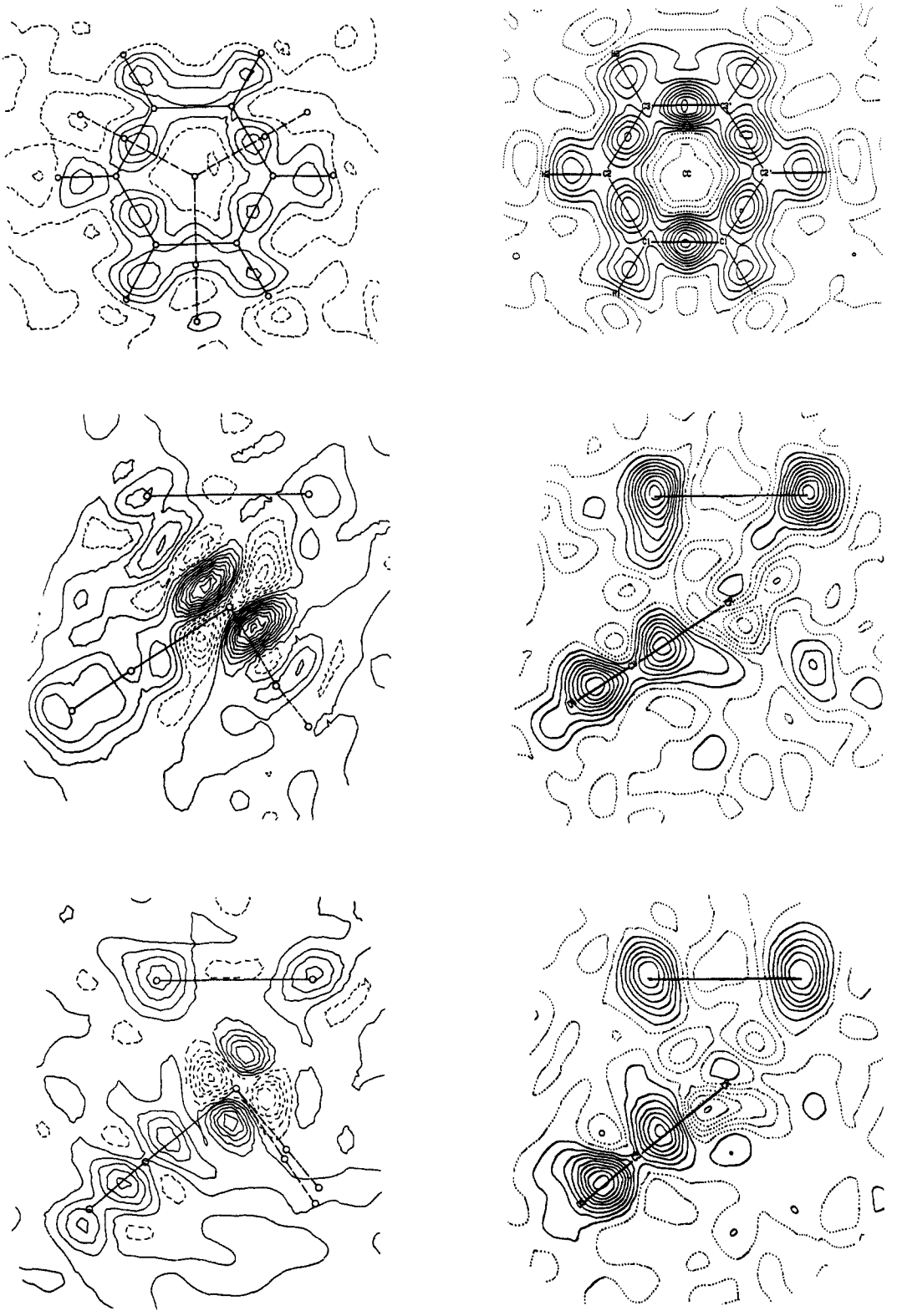

Figure 4. Experimental deformation density maps. Those on the left are from Rees and Coppens and are contoured at 0.15 e $Å^{-3}$. Those on the right are from Molecular Structure Corp. and are contoured at 0.05 e $Å^{-3}$.

of the benzene ring as in our theoretical maps, and there is a weak pattern of loss which resembles the theoretical maps. However, the differences between our theoretical and these experimental maps around Cr is substantial.

Fragment Deformation Density Maps. We have further investigated the electron distribution and bonding in $Cr(C_6H_6)(CO)_3$ by examining several fragment deformation density maps. As was mentioned earlier, deformation density maps are usually produced by subtracting the superposition of the best spherical, ground-state atoms from the theoretical electron density distribution. Interpretation of both theoretical and experimental results is sometimes difficult, however, because changes in the atomic electron distributions may mask more subtle changes due to fragment interaction. For example, changes in one region of the molecule may be caused by changes occurring in several other places in the molecule. It is difficult to separate all these effects when dealing with atomic deformation densities.

This problem can be minimized by subtracting the theoretical densities of the molecular fragments from the total density of the complex. Since both the complex and the fragments are calculated

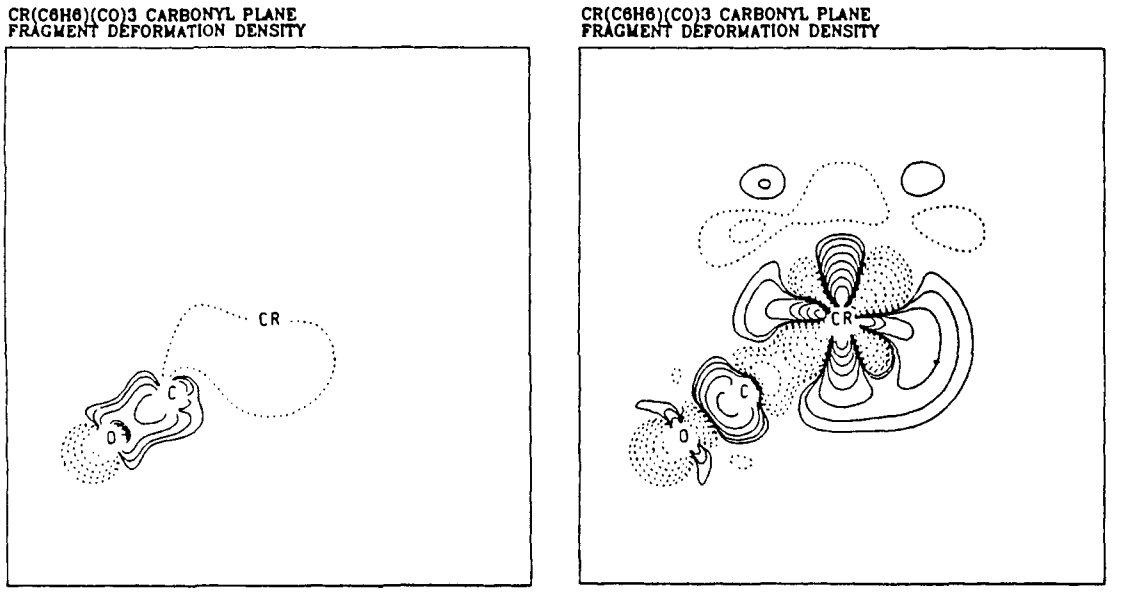

Figure 5. Fragment deformation density maps for $Cr(C_6H_6)(CO)_3$. The outermost contour has a value of 1/512 e au^{-3} or 0.013 e Å^{-3}. This solid or dotted line represents the smallest positive or largest negative contour, respectively. Adjacent contours differ by a factor of 2.

within the same limitations of the basis set and calculational method chosen, most errors involved are cancelled upon computing the deformation density. Furthermore, each fragment has already incorporated the gross electron density shifts associated with internal bond formation into its electron density, and so the fragment deformation density maps tend to reflect the less obvious density changes which occur both at the interface of the fragments during complexation as well as within those fragments after complexation. Finally, the fragment deformation density approach lets one selectively examine the deformation density on forming certain bonds without interference from the formation of other bonds.

Two fragment deformation density maps are shown in Figure 5. In contrast to the other maps shown in this paper which have linearly spaced contours, these maps have contours plotted in a geometric relationship with adjacent contours differing from each other by a factor of 2. On the left side of Figure 5, we have plotted a map which shows the interaction of the benzene ring with the carbonyl groups. This map was generated by calculating the density of a system containing a benzene ring and three carbonyls at their equilibrium positions but with no chromium atom and then subtracting the electron density of free benzene and CO. If the carbonyls had any direct interaction with the benzene ring, one would expect to see changes in the electron density in the region at the top of this map. Instead this part of the map is blank, indicating that the electron distribution of the benzene in this system is equal with that in free benzene. The same cannot be said for the carbonyl region. Here one sees that subtracting the density of free CO does not give a blank area but rather gives a small change in the deformation density. The innermost contour between the carbon and the oxygen has a value of 0.11 e Å^{-3} so this change is small, but it does indicate that the CO groups interact directly with each other. This is due to their proximity to each other and because the pyramidal arrangement points the p orbitals toward the same general region of space.

On the right side of Figure 5, we have plotted a map which examines the interaction of the chromium and the ligand system. This map was generated by subtracting the electron density of a free benzene, three carbonyls, and a lone chromium atom from the total electron density of the molecule. From the large buildup of electron density between the carbon and the chromium shown in Figure 3, one might infer strong chromium–carbon interaction. However, this fragment map shows that this buildup is almost entirely due to the carbon lone-pair formation not to C–Cr bond formation. When free carbon monoxide is subtracted, this region in fact ends up negative. This can be understood by considering the chromium to be in an octahedral ligand field. In such a field, the normally spherical electron density distribution will rearrange so that electron density will flow out of d orbitals that point directly toward the incoming ligands. Thus, the deformation density in this region will be negative since you are subtracting a spherical atom which has density in this region from a molecule in which density has been removed from this region. Near the carbon one sees loss due to donation from carbonyl to metal. Elongation of the electron density perpendicular to the bond axis on the carbonyl indicates that chromium–carbonyl interaction does lead to build up in the carbonyl π region.

Conclusion

The results show that a number of problems still exist with experimental electron deformation density studies on $Cr(C_6H_6)(CO)_3$. The two experimental studies on $Cr(C_6H_6)(CO)_3$ differ significantly from each other. Information about the electron distribution close to the chromium may be unreliable due to the large number of electrons in the core. In both this theoretical study and Rees and Coppens' experimental study, the largest changes in the electron density distribution are around the chromium atom. However, the difference in the pattern of electron gain and loss around the chromium is difficult to explain. Perhaps the peaks in the experimental study are distorted by contributions from "ghost peaks". The reason for lack of density around the Cr in the Troup and Extine study is also not obvious. Finally, in spite of our overestimation of the O lone pair, we believe the O lone-pair regions on the experimental maps are underestimated.[10]

In conclusion, this study has presented a simple method of incorporating thermal smearing into theoretical static deformation densities. The fragment deformation density has been used to examine the electron density distribution in $Cr(C_6H_6)(CO)_3$ and has helped to explain the deformation density maps in simple chemical terms. Although problems still exist in the experimental studies of this molecule, our work has shown that accurate calculations can aid in the interpretation of experimental deformation densities.

Acknowledgment. This work was supported by the National Science Foundation (CHE79-20993, CHE83-09936) and the Robert A. Welch Foundation (A-648). The Department of Chemistry's VAX 11/780 was purchased in part through a major instrument grant from the National Science Foundation (CHE80-15792).

Registry No. $Cr(C_6H_6)(CO)_3$, 12082-08-5.